IEEE Access
Multidisciplinary ⋮ Rapid Review ⋮ Open Access Journal

Received September 6, 2019, accepted October 16, 2019, date of publication October 22, 2019, date of current version November 4, 2019.

Digital Object Identifier 10.1109/ACCESS.2019.2948823

A Compact Antenna for GPS Anti-Jamming in Airborne Applications

NAVID REZAZADEH, (Member, IEEE), AND LOTFOLLAH SHAFAI, (Life Fellow, IEEE)
Department of Electrical and Computer Engineering, University of Manitoba, Winnipeg, MB R3T5V6, Canada
Corresponding author: Navid Rezazadeh (navid.rezazadeh@umanitoba.ca)

ABSTRACT Null-steering using adaptive antenna systems is a robust method to global positioning system (GPS) receivers against hostile jamming. Conventionally, multi-antenna arrays have been utilized for such receivers, but the size and weight are often prohibitive especially for space-limited airborne applications. In this paper, we present another approach based on antenna pattern and polarization diversity to enable null-steering, and propose a design with co-located elements to achieve a small footprint. As a proof-of-concept, we present an antenna prototype with a size of only $5 \times 5 \times 1.9$ cm^3 ($0.26\lambda \times 0.26\lambda \times 0.1\lambda$) at the L1 band, capable of steering two nulls. We present the simulated and measured parameters of the antenna, study its null-steering performance in various interference scenarios with a simple power minimization method, and demonstrate its capability in suppressing up to two jamming signals incident from the angular region close to horizon.

INDEX TERMS Adaptive antennas, global positioning system, interference suppression.

I. INTRODUCTION

Global positioning system (GPS) has enabled and augmented many technologies in different sectors by providing navigation and timing information. It also has an indispensable role in the navigation and safety of manned and unmanned aircraft. The satellite signals are however very weak, making them specifically vulnerable to radio frequency (RF) interference, and unsurprisingly, due to the high reliance of many sensitive applications on GPS, this issue has been studied extensively.

The source of interference could be unintentional, such as signals in the same band or harmonics of out-of-band signals usually originating from sources close to a GPS receiver. The interference could also be intentional, such as hostile jamming, in which case a high power signal is transmitted in the same band to overwhelm the receiver and raise the noise level to degrade its performance or completely thwart its operation. The jamming signal waveform could take different forms such as narrowband, wideband or swept-frequency [1].

Different techniques have been developed to combat GPS jamming. Filtering in time and frequency domains are usually the first step, but they have their own limitations especially against wideband jamming signals. Spatial filtering adds another level of defense, which is specifically useful against wideband jamming [2]. A fixed-type spatial filter can be implemented by antennas equipped with ground-chokes for example, to suppress the unwanted signals originating from below horizon [3], but this technique also to some extent suppresses the desired satellite signals close to horizon. Adaptive spatial filtering overcomes this limitation by adapting the receive antenna pattern in real-time to combat jamming, and is therefore a much more robust and versatile technique than the fixed spatial filtering. It is conventionally implemented by multi-antenna systems, in which by properly weighting the signals received by each antenna element, a null is formed in the pattern at the direction of a jamming signal to suppress it in real time. These types of antennas are referred to as controlled reception pattern antennas (CRPAs).

The requirement for anti-jamming CRPAs are light weight, small size and good null-steering performance [4]. Planar arrays of microstrip or spiral antennas are the most common type of compact CRPAs developed to date [5] but they often face a challenge in meeting the requirements. This is because there is often a direct trade-off between the array performance and array size (and thus element spacing). It is known that half-wavelength element spacing is ideal in an antenna array, but this is prohibitively large for the L-band GPS signals and therefore most modern GPS arrays are designed with much smaller element spacing, in the order of $0.15-0.3\lambda$ [5]. As an example, a four-element microstrip patch antenna array with a total size of $11.7 \times 11.7 \times 1.1$ cm^3 ($0.48\lambda \times 0.48\lambda \times 0.05\lambda$

The associate editor coordinating the review of this manuscript and approving it for publication was Yunlong Cai.

at L2 band) was reported in [6]. Reducing the array size below such a small size by reducing the element spacing even further would lead to high levels of mutual coupling and a degradation in the null-steering performance of the array due to a lower spatial resolution.

To implement spatial filtering within a ultra-small footprint, we take a different approach in this work. Instead of utilizing an antenna array with similar element patterns, which relies on the diversity in the location of phase centers of its element to collect different samples of an incoming plane wave signal for beamforming and null-steering, we use multiple antenna elements with the same phase center but with different polarization and patterns to implement null-steering. Such a technique was used in [7] using co-located higher-order modes of TM_{n1}, $(n = 1, 2, 3, 4)$ microstrip patch antennas for beamforming in the horizontal plane. The same higher-order modes of microstrip antennas were used later for null-steering as well. In [8], a $TM_{11} - TM_{21}$ microstrip antenna geometry was designed for satellite receive applications, capable of steering one null. However, the antenna is printed on low dielectric constant material and the TM_{21} mode is excited by a shorted ring on a ground plane, resulting in a prohibitively large overall antenna size of 20 cm diameter (1.05λ). Another similar design with $TM_{11} - TM_{21} - TM_{31}$ modes was presented in [9] but still with a prohibitively large size (1.6λ diameter) for compact platforms. The issue of size was addressed in [10] where a $TM_{11} - TM_{21}$ microstrip patch antenna was presented where both modes are excited in rings (as opposed to shorted rings) and on a higher dielectric constant substrate, achieving a compact diameter of 6.4 cm at the GPS L1 band (0.33λ). Furthermore, both polarizations of each element were utilized independently in this design, enabling the steering of up to three nulls. Due to the extreme miniaturization however, the bandwidth of this antenna is small (5 MHz) and only sufficient for the reception of the coarse acquisition (C/A) signal.

In all of the aforementioned designs, the first dominant mode provides a broadside pattern with maximum at zenith, while the higher order modes provide conical patterns with a null at zenith and a maximum closer to horizon. This diversity in patterns therefore, enables null-steering at angles close to horizon. However, the issue with utilizing multi-mode microstrip patch antennas in co-centered geometries is the high quality factor of the higher-order modes which results in either a large antenna size for the required bandwidth [8], [9], or a very small bandwidth if the antenna is miniaturized [10]. In this work, we utilize a microstrip antenna to produce a first mode with a typical broadside pattern, but instead of using higher-order modes of microstrip antennas, we utilize a miniaturized monopole to obtain the auxiliary omni-directional pattern. Furthermore, to maximize the degrees of freedom of the antenna, we use both orthogonal polarizations of the microstrip antenna independently. We miniaturize both the microstrip and monopole elements to achieve a small size while maintaining more than 30 MHz bandwidth at the L1 band which covers the P(Y) and M signals as well as the legacy C/A signal. Finally, we show that the antenna is capable of nulling up to two jammers incident from low elevation angles.

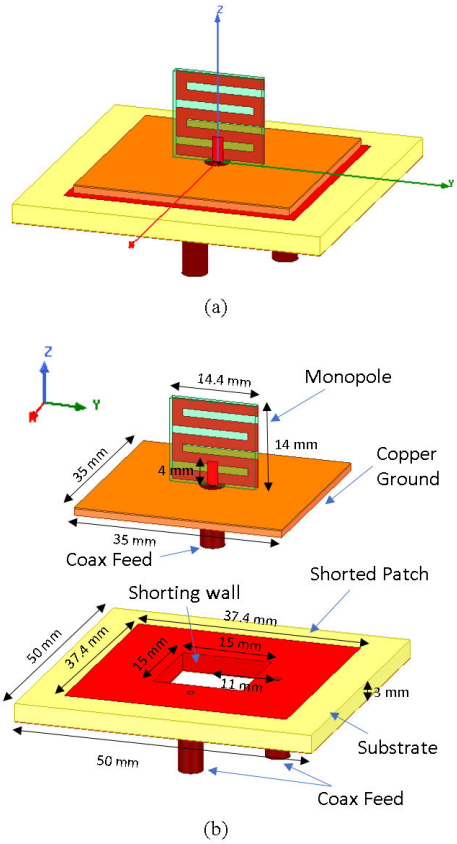

FIGURE 1. (a) The geometry of the proposed GPS anti-jamming antenna. (b) The exploded view.

The paper is organized as follows. The antenna geometry and its simulated and measured parameters are given in section II and the interference suppression analysis using the antenna is presented in section III.

II. ANTENNA DESIGN AND CHARACTERIZATION

The geometry of the antenna is shown in Fig. 1 (a), with the exploded view and dimensions shown in Fig. 1 (b). The antenna is modeled and simulated in ANSYS HFSS. A spherical coordinate system is assumed throughout the paper with the z-axis aligned to zenith and the x-y plane as horizon. The antenna consists of two elements, a square patch at the bottom and a monopole on the top. The square patch's dimensions are adjusted for operation of the dominant TM_{01} mode, which has a broadside gain pattern with its maximum at zenith, as is most common in GPS microstrip antennas. Two coaxial lines feed this element at 90° angle for the two orthogonal polarizations (x and y) which in this case are independent, rather than being combined by a hybrid coupler to get right-hand circular polarization (RHCP). This adds an additional degree of freedom for null-steering.

The substrate chosen for the patch element is a 3 mm thick Rogers AD1000 with a dielectric constant of $\epsilon_r = 10.2$ and loss tangent of $\delta = 0.0023$ which are common values for

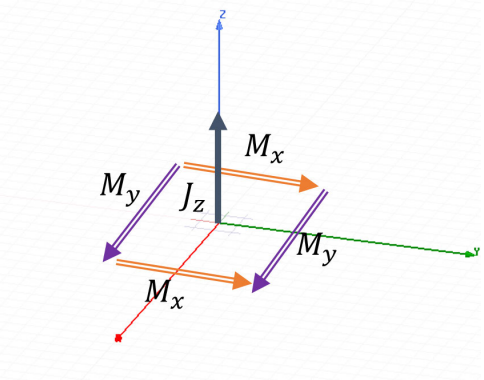

FIGURE 2. The equivalent current source representation of the antenna of Fig. 1.

GPS antennas. The patch element is different compared to common GPS patch antennas however, in that the patch is shorted at the center and the middle part of the substrate is completely removed. This provides a small opening to feed the monople element which sits on top. We note that the size of this element could be further miniaturized using a higher dielectric constant substrate.

The element sitting on top is a monopole consisting of a meandered radiating element fed capacitively by a vertical strip to achieve miniaturzation. This element is based on a metamaterial-inspired antenna designed in [11]. Since a detailed analysis is provided in [11], it will not be repeated here and interested readers are referred to the original work. The monopole height is 14 mm, which is 0.07λ at the L1 band center frequency (1.575 GHz). For simple fabrication, the monopole is printed on a substrate with the meander line on one side and the feed strip on the other side. For this element, a substrate of Rogers RO3010 with dielectric constant of $\epsilon_r = 10.2$ and loss tangent of $\delta = 0.0035$ was chosen. In this case a higher value of substrate permittivity will not actually provide any significant miniaturization as most of the near fields of the antenna are not confined within the substrate. Since the monopole is sitting on top of the patch, its ground plane size is chosen just to be smaller than the patch underneath to not block the radiation of the patch.

Even though both the patch and the monople are radiating from the same phase center, their mutual coupling can be made very small thanks to their different radiation patterns. This can be shown analytically as follows. First, the antenna model is represented by equivalent current sources, as shown in Fig. 2. As such, the monopole antenna is represented by a vertical electric current source, whereas the patch antenna is represented by two pairs of horizontal magnetic current sources for the x and y polarizations. The former representation is according to the cavity model of a patch antenna which states that the radiation of a rectangular patch originates from the fringing fields at the two ends of the patch much like an array of two slot antennas. Given that the dimensions of the elements in the design are much smaller than the free space wavelength, we assume the currents are all uniform in amplitude and phase. With these assumptions and using the concept of electric and magnetic vector potentials [12, p. 143], the far-field patterns of each element can be found as

$$\vec{f}_{px}(\theta,\phi) = f_{px0}(-cos\phi\ \hat{\theta} + cos\theta sin\phi\ \hat{\phi}) \times \frac{sin(k\frac{a}{2}sin\theta sin\phi)}{sin\theta sin\phi} cos(k\frac{a}{2}sin\theta cos\phi) \quad (1a)$$

$$\vec{f}_{py}(\theta,\phi) = f_{py0}(sin\phi\ \hat{\theta} + cos\theta cos\phi\ \hat{\phi}) \times \frac{sin(k\frac{a}{2}sin\theta cos\phi)}{sin\theta cos\phi} cos(k\frac{a}{2}sin\theta sin\phi) \quad (1b)$$

$$\vec{f}_{m}(\theta,\phi) = f_{m0}(sin\theta\ \hat{\theta}) \frac{sin(k\frac{l}{2}cos\theta)}{cos\theta} \quad (1c)$$

for the x and y polarization patterns of the patch, and the monopole respectively. In the expressions above, a is the side length of the square patch (or more precisely, the effective length with the fringing fields taken into account), l is the length of the monopole and k is the wavenumber in free space. Furthermore, the constants f_{px0}, f_{py0} and f_{m0} can be chosen such that the expressions above are the directivity values such that

$$\int_0^{2\pi}\int_0^{\pi} \vec{f}(\theta,\phi)\cdot\vec{f}^*(\theta,\phi)\ sin\theta d\theta d\phi = 4\pi. \quad (2)$$

This is done only to be able to compare the patterns with one another and the absolute values of the constants are not important for this analysis.

The mutual coupling of two antennas are related to their far-field patterns through the concept of generalized radiation scattering parameters, in which a parameter called beam coupling factor is defined as a measure of the similarity between any two antenna radiation patterns as [13]

$$\beta(\vec{f}_1,\vec{f}_2) = \frac{1}{4\pi}\int_0^{2\pi}\int_0^{\pi} \vec{f}_1(\theta,\phi)\cdot\vec{f}_2^*(\theta,\phi)\ sin\theta d\theta d\phi \quad (3)$$

It has a value between 0 and 1 from completely orthogonal patterns to completely similar patterns respectively. A low coupling factor is a necessary condition for low mutual coupling but not a sufficient one, i.e. if $|\beta|$ is low between the patterns of two antennas, low mutual coupling between them can in principle be achieved although it is not guaranteed. On the other hand, low mutual coupling cannot be achieved between two antennas if their beams have a high coupling factor. The beam coupling factor for the case of a patch and a monopole is shown in Fig. 3 (a) as a function of the distance between their phase centers. For comparison, the beam coupling factor between two patches are also given in Fig 3 (b). As it is shown, the coupling factor between a co-centric patch and monople is very low when their phase centers coincide. This is in contrast with conventional arrays with similar elements, in which as shown in Fig 3 (b) the beam coupling factor is maximum for co-located antennas and only becomes small when the inter-element spacing is approximately half a wavelength.

It is noted here that even though the patterns of the patch and monopole have a low beam coupling factor, they still have sufficient overlap to allow null-steering at the angular region close to horizon. This will be shown in more detail in section III.

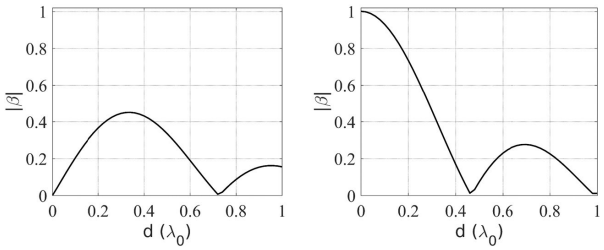

FIGURE 3. The beam coupling factor as a function of distance between two antennas (a) A monopole and a patch. (b) Two patches.

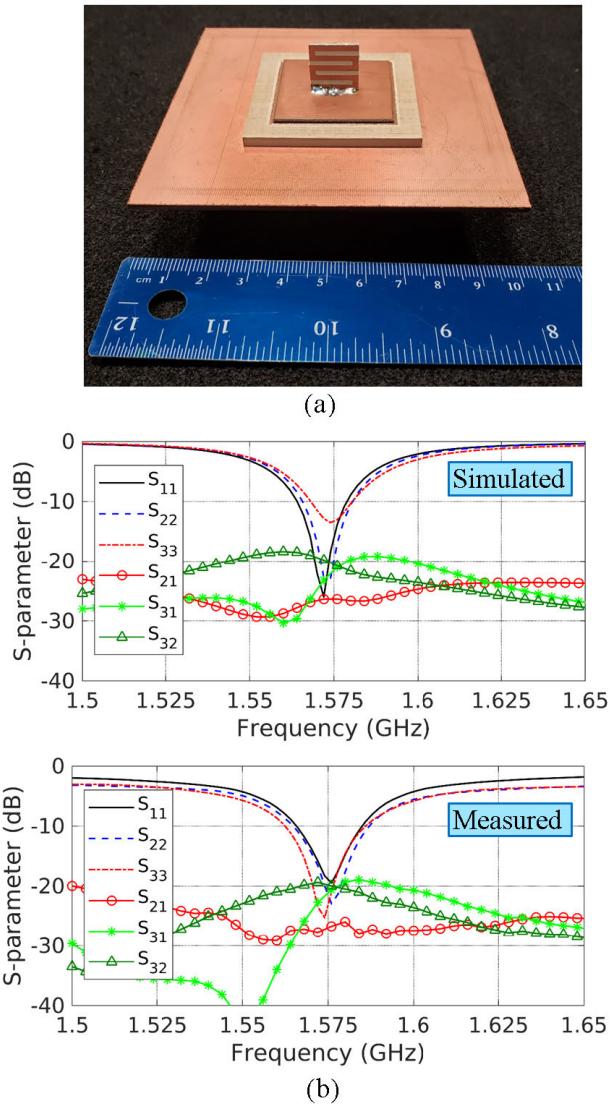

FIGURE 4. (a) The fabricated antenna. (b) The simulated S-parameters. (c) The measured S-parameters.

To antenna was fabricated using an LPKF milling machine and manual soldering and assmebly. The final design is shown in Fig. 4 (a). Due to the very small ground plane of the antenna, a slightly larger conducting plate of size 10 cm was added to the antenna as backing which provides support for installation on the radiation pattern measurement mast, and reduces the effect of cable radiation and scattering which occurs in measurements of antennas with small ground planes. The S-parameters of the antenna were measured using a Keysight vector network analyzer. The simulated and measured S-parameters are shown in Fig. 4 (b), showing good agreement between them. The port for the x and y polarized patch are labeled 1 and 2 respectively, and the port for the monopole is labeled 3. The measured -10 dB return loss bandwidth of both elements are more than 25 MHz, and the mutual coupling between all ports remain below -18 dB, which is very low and consistent with the analysis given earlier.

The antenna's radiation patterns were measured in a compact range at the University of Manitoba, with the setup shown in Fig. 5 (a). The simulated and measured results are given in Fig 5 (b). The agreement between the simulation and measurement is fairly good for both the patch and monople cases, but larger errors are noticeable in the monopole case. This is mostly due to the small ground plane and conducting backing used in the design, which do not completely eliminate the cable effects on the measurements. To further reduce the cable effects, baluns and ferrite beads are usually placed on the cable very close to the antenna feeding point [14].

The simulated and measured peak gains of the antenna elements as a function of frequency are shown in Fig. 5 (c). The patch has a typical peak gain of around 5 dBi and the monopole has a peak gain of 0 dBi. The measured gains have less than 2 dB variation throughout a 30 MHz bandwidth, which is sufficient for the reception of all GPS L1 band signals.

III. INTERFERENCE SUPPRESSION PERFORMANCE

We now utilize a numerical approach to look at how the proposed antenna can steer nulls to suppress jamming. For simplicity, we assume all the signals to be single tone but the results will be general if the RF front-ends are not too frequency dispersive, otherwise some finite impulse response (FIR) filters can be placed at the input of each antenna to compensate for the frequency dependence of the RF front-end responses [4]. The signals received by each antenna channel feed into an adaptive processing unit, which could be implemented at the analog or digital level. Each signal is multiplied by some complex weight and summed at the output of the adaptive processing unit.

The proposed antenna has three independent channels and so it can cancel up to two jammers, but the formulation will be given for a general case of an N-channel antenna and M incident signals. Assume that M plane wave signals, some desired and some jammers, are incident on the array from angles (θ_m, ϕ_m) with polarization-phase vectors $\hat{e}_m$ and amplitude A_m which is assumed to be a Gaussian random variable $\mathcal{N}(0, \sigma_m)$. The antenna response vector to each incident plane wave signal is $\boldsymbol{x}_m \in \mathcal{C}^{N\times 1}$ written as

$$\boldsymbol{x}_m = \begin{bmatrix} A_m \vec{f}_1(\theta,\phi)\cdot\hat{e}_m \\ A_m \vec{f}_2(\theta,\phi)\cdot\hat{e}_m \\ \cdots \\ A_m \vec{f}_N(\theta,\phi)\cdot\hat{e}_m \end{bmatrix}, \tag{4}$$

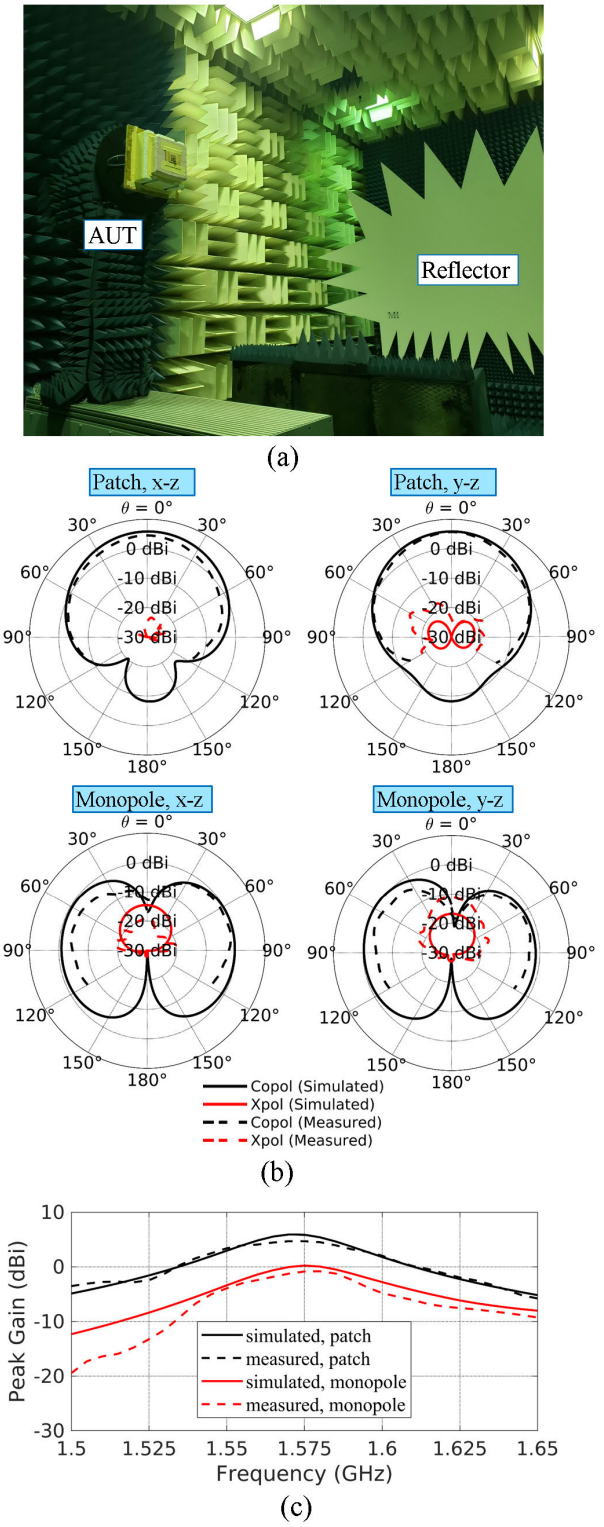

FIGURE 5. (a) The pattern measurement setup of the antenna in a compact range. (b) The simulated and measured gain patterns. (c) Antenna peak gains as a function of frequency.

the total response is the summation of (4) over all incident signals

$$\boldsymbol{x} = \sum_{m=1}^{M} \boldsymbol{x}_m \tag{5}$$

and the output of the adaptive array is

$$y = \boldsymbol{w}^H \boldsymbol{x} \tag{6}$$

where $\boldsymbol{w} \in \mathcal{C}^{N\times 1}$ is the vector of complex weights and superscript H denotes the Hermitian operation. The goal of the adaptive processor is to adjust the complex weights in real-time using an algorithm to suppress the interference signals at the output. Various adaptive interference canceling techniques exist which depend on various forms of a priori information available to the receiver and the receiver's processing capabilities. These methods are out of the scope of this paper and can be found for example in [15]. In this paper, we utilize a very simple but effective nulling approach called power minimization, where the complex weights are found such that the overall power at the output is minimized subject to a linear constraint [16]. To simplify the method further, the linear constraint is chosen as a desired quiescent pattern of the antenna in the absence of any interference. In this case, the most appropriate quiescent pattern is when only the patch antenna is active and is in RHCP mode, so the constraint vector is $\boldsymbol{w}_c = [1\ j\ 0]^T$.

In the presence of interference, the weight vector is updated to

$$\boldsymbol{w}_{opt} = \alpha \boldsymbol{R}^{-1} \boldsymbol{w}_c \tag{7}$$

in which α is an inconsequential scalar, and $\boldsymbol{R}$ is the covariance matrix of the input signal, given by

$$\boldsymbol{R} = E\{\boldsymbol{x}\boldsymbol{x}^H\} + \sigma_n^2 I_N \tag{8}$$

in which $E\{\}$ is the expected value, σ_n^2 is the thermal noise power, and I_N is the identity matrix.

Note that this adaptive method suppresses any signals that are higher than the noise level, which is specifically suitable for the GPS application where the desired satellite signals are buried in noise but jamming signals are usually higher than noise. The advantage of this method is its simplicity, since it does not require any a priori knowledge of the desired or interference signals.

We are now finally ready to study the jammer suppression of the proposed antenna. To implement the power minimization method, first the 2-D radiation patterns of the antenna are exported from HFSS to MATLAB, where the optimum weights are computed based on the power minimization method and then the optimum weights are exported from MATLAB back to HFSS in order to validate the nulling scheme, and obtain a visual representation of the adapted pattern. The weight vector is always normalized such that $|\boldsymbol{w}| = 1$, and the jammer power is assumed to be 20 dB higher than the noise level, i.e. interference-to-noise ratio (INR) at the adaptive antenna input is 20 dB.

First, we look at the antenna response when there are no jammers. The adapted pattern in this case is simply the antenna quiescent pattern shown in Fig. 6 (a) in two representations. The representation on the left is the 3-D polar pattern from HFSS where the coordinate system is specified, and the

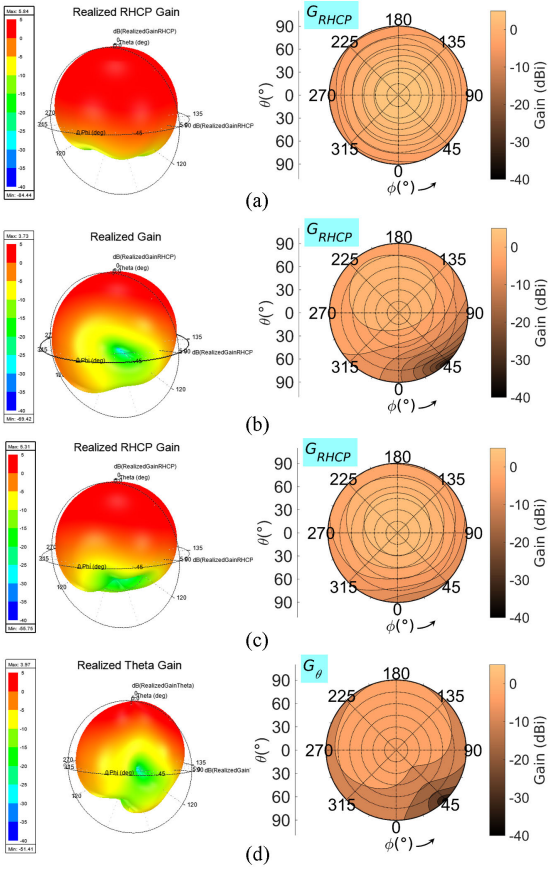

FIGURE 6. (a) The antenna quiescent pattern in the absence of interference. (b) Antenna's adapted RHCP gain for one RHCP jammer at $(\theta, \phi) = (90°, 45°)$. (c) Antenna's adapted RHCP gain and (d) θ gain for a vertically-polarized jammer at $(\theta, \phi) = (90°, 45°)$.

one on the right is a 2-D polar plot produced in MATLAB which shows the antenna pattern from the top, i.e. the center of the plot is zenith and the perimeter is horizon.

As a first jamming example, we assume a single RHCP jammer is incident from an angle $(\theta, \phi) = (90°, 45°)$. The RHCP component of the adapted pattern of the antenna is given in Fig. 6 (b), which shows a deep null at the direction of the jammer. In this case, the output INR is -18 dB, indicating a jammer suppression of 38 dB.

For the second jamming example, we keep the jammer direction unchanged but assume a linear vertical polarization for it this time. Fig. 6 (c) shows the RHCP component of the adapted pattern which does not show a deep null in this case. This is because the proposed antenna is polarization diverse and therefore only needs to suppress the polarization component corresponding to that of the jammer. So in this case the null is only placed in the θ component of the adapted pattern, as shown in Fig. 6 (d). In other words, the adaptive antenna taylors its response not only with respect to the direction of the jammer, but also its polarization. The nulling in this case suppressed the jammer to 15 dB below noise (output INR of -15 dB).

Finally, we look at an example with two jammers incident from angles $(\theta_1, \phi_1) = (90°, 45°)$ and

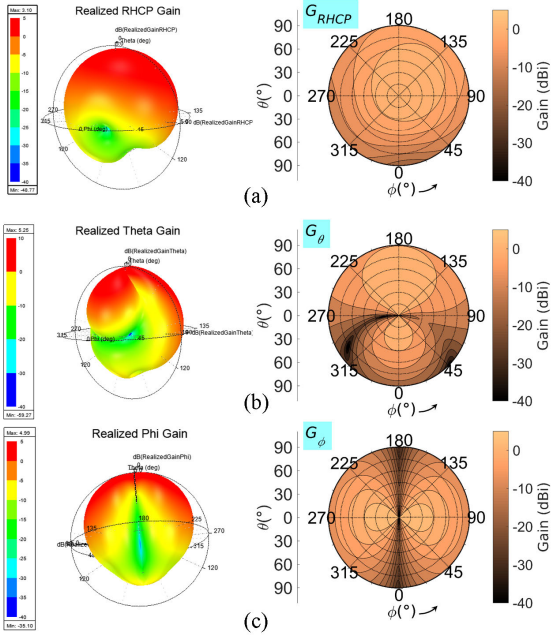

FIGURE 7. Antenna's adapted (a) RHCP gain, (d) θ gain, and (c) ϕ gain for one vertically-polarized jammer at $(\theta, \phi) = (90°, 45°)$ and one horizontally-polarized at $(\theta_2, \phi_2) = (110°, 180°)$.

$(\theta_2, \phi_2) = (110°, 180°)$. The first is assumed to be vertical, and the second is assumed to be horizontal. Note that the second jammer originates from below the horizon, simulating a practical scenario in an airborne application. Various components of the adapted antenna pattern are shown in Fig. 7. (a)-(c). The θ and ϕ components each show a null corresponding to each jammer, whereas the RHCP pattern does not have any deep nulls, therefore improving the chance of reception from satellites even while null-steering. The jammers are suppressed to 12 dB below the noise floor in this case (output INR of -12 dB).

IV. CONCLUSION

A compact antenna for GPS anti-jamming application was designed and studied. The antenna consists of a dual-polarized patch and a monopole radiating from the same phase center which due to the diversity of their patterns have very low mutual coupling. It was shown that despite the small footprint of the antenna compared to conventional larger arrays, by combining the signals of each channel of the antenna with appropriate weights, null-steering similar to conventional larger arrays can be achieved. With a total size of only 0.26 λ, this antenna can cancel up to 2 jammers incident from low elevation angles.

Further improvements can be made in the antenna geometry as follows. First, using a higher dielectric constant, the patch element could be made smaller. Second, the hollowed section of the patch can be made much smaller by choosing a smaller coaxial feeding for the monopole element on top (e.g. U.FL connectors instead of SMA), resulting in further miniaturization of the patch element. Third, both of the patch and monopole elements can be made multi-band

using well-known techniques for multi-band GPS/GNSS receivers.

REFERENCES

[1] M. Trinkle and D. Gray, "Gps interference mitigation; overview and experimental results," in *Proc. 5th Int. Symp. Satell. Navigat. Technol. Appl.*, Canberra, Australia, 2001, pp. 1–14.

[2] R. T. Ioannides, T. Pany, and G. Gibbons, "Known vulnerabilities of global navigation satellite systems, status, and potential mitigation techniques," *Proc. IEEE*, vol. 104, no. 6, pp. 1174–1194, Jun. 2016.

[3] J. Tranquilla, J. P. Carr, and H. M. Al-Rizzo, "Analysis of a choke ring groundplane for multipath control in Global Positioning System (GPS) applications," *IEEE Trans. Antennas Propag.*, vol. 42, no. 7, pp. 905–911, Jul. 1994.

[4] I. J. Gupta, I. M. Weiss, and A. W. Morrison, "Desired features of adaptive antenna arrays for GNSS receivers," *Proc. IEEE*, vol. 104, no. 6, pp. 1195–1206, Jun. 2016.

[5] J. L. Volakis, A. J. O'Brien, and C.-C. Chen, "Small and adaptive antennas and arrays for GNSS applications," *Proc. IEEE*, vol. 104, no. 6, pp. 1221–1232, Jun. 2016.

[6] M. Chen and C.-C. Chen, "A compact dual-band GPS antenna design," *IEEE Antennas Wireless Propag. Lett.*, vol. 12, pp. 245–248, 2013.

[7] L. Shafai, "Linear-sum mode arrays and beam forming," in *Proc. Symp. Antenna Technol. Appl. Electromagn.*, Aug. 1992, pp. 57–62.

[8] N. R. Labadie, S. K. Sharma, and G. M. Rebeiz, "A circularly polarized multiple radiating mode microstrip antenna for satellite receive applications," *IEEE Trans. Antennas Propag.*, vol. 62, no. 7, pp. 3490–3500, Jul. 2014.

[9] B. Babakhani and S. K. Sharma, "Dual null steering and limited beam peak steering using triple-mode circular microstrip patch antenna," *IEEE Trans. Antennas Propag.*, vol. 65, no. 8, pp. 3838–3848, Aug. 2017.

[10] N. Rezazadeh and L. Shafai, "A compact microstrip patch antenna for civilian GPS interference mitigation," *IEEE Antennas Wireless Propag. Lett.*, vol. 17, no. 3, pp. 381–384, Mar. 2018.

[11] A. Erentok and R. W. Ziolkowski, "Metamaterial-inspired efficient electrically small antennas," *IEEE Trans. Antennas Propag.*, vol. 56, no. 3, pp. 691–707, Mar. 2008.

[12] C. A. Balanis, *Antenna Theory: Analysis and Design*. Hoboken, NJ, USA: Wiley, 2016.

[13] A. Ludwig, "Mutual coupling, gain and directivity of an array of two identical antennas," *IEEE Trans. Antennas Propag.*, vol. AP-24, no. 6, pp. 837–841, Nov. 1976.

[14] C. Icheln, J. Krogerus, and P. Vainikainen, "Use of balun chokes in small-antenna radiation measurements," *IEEE Trans. Instrum. Meas.*, vol. 53, no. 2, pp. 498–506, Apr. 2004.

[15] C. Fernández-Prades, J. Arribas, and P. Closas, "Robust GNSS receivers by array signal processing: Theory and implementation," *Proc. IEEE*, vol. 104, no. 6, pp. 1207–1220, Jun. 2016.

[16] O. L. Frost, III, "An algorithm for linearly constrained adaptive array processing," *Proc. IEEE*, vol. 60, no. 8, pp. 926–935, Aug. 1972.

NAVID REZAZADEH (S'11–M'18) received the B.Sc. degree from the University of Tehran, Tehran, Iran, in 2011, and the M.Sc. and Ph.D. degrees from the University of Manitoba, Winnipeg, Canada, in 2014 and 2018, respectively.

Since 2018, he has been a Postdoctoral Fellow with the Department of Electrical and Computer Engineering, University of Manitoba, and a Technical Research Lead with HaiLa Tech., Montreal, QC, Canada. He has published several journals and conference papers and serves as a Reviewer for multiple IEEE journals. His current research interests include antennas, applied electromagnetics, and digital communication systems.

Mr. Rezazadeh received two Student Paper Awards from the IEEE Antennas and Propagation Society and the International Union of Radio Scientists, in 2017, for his work on advanced anti-jamming GPS antennas. He was a recipient of the Graduate Fellowship from the University of Manitoba, in 2015.

LOTFOLLAH SHAFAI (LF'07) received the B.Sc. degree from the University of Tehran, in 1963, and the M.Sc. and Ph.D. degrees from the University of Toronto, in 1966 and 1969, respectively. In 1969, he joined the Department of Electrical and Computer Engineering, University of Manitoba, as a Lecturer, an Assistant Professor, in 1970, an Associate Professor, in 1973, a Professor, in 1979, a Distinguished Professor, in 2002, and a Distinguished Professor Emeritus, in 2016. His assistance to industry was instrumental in establishing an Industrial Research Chair in applied electromagnetics with the University of Manitoba, in 1989, which he held until 1994. In 1986, he established the symposium on Antenna Technology and Applied Electromagnetics, ANTEM, with the University of Manitoba, which has grown to be the premier Canadian conference in antenna technology and related topics. In 2002, he was elected as a Fellow of The Canadian Academy of Engineering and a Distinguished Professor of The University of Manitoba. In 2009, he was elected as a Fellow of the Engineering Institute of Canada. He is a Life Fellow of the Royal Society of Canada. He has been a recipient of numerous awards. In 1978, his contribution to the design of the first miniaturized satellite terminal for the Hermes satellite was selected as the Meritorious Industrial Design. In 1984, he received the Professional Engineers Merit Award and the The Thinker Award from the Canadian Patents and Development Corporation, in 1985. From the University of Manitoba, he received the Research Awards in 1983, 1987, and 1989, the Outreach Award, in 1987, and the Sigma Xi Senior Scientist Award, in 1989. In 1990, he received the Maxwell Premium Award from IEE, London, and the Distinguished Achievement Awards from Corporate Higher Education Forum, in 1993 and 1994, respectively. In 1998, he received the Winnipeg RH Institute Foundation Medal for Excellence in Research. In 1999 and 2000, he received the University of Manitoba Research Award. He was a recipient of the IEEE Third Millennium Medal, in 2000. In 2003, he received an IEEE Canada Reginald A. Fessenden Medal for Outstanding Contributions to Telecommunications and Satellite Communications, and the Natural Sciences and Engineering Research Council (NSERC) Synergy Award for Development of Advanced Satellite and Wireless Antennas. He held a Canada Research Chair 2001–2016 in applied electromagnetics and was the International Chair of Commission B of the International Union of Radio Science (URSI) for 2005–2008. He was a recipient of the IEEE Chen-To-Tai Distinguished Educator Award, in 2009. In 2011, he received the Killam Prize in engineering from The Canada Council, for his outstanding Canadian career achievements in engineering, and his research on antennas. In 2013, he received the John Kraus antenna Award from the IEEE Antennas and Propagation Society for the contributions to the design and understanding of small high efficiency feeds and terminals, wideband planar antennas, low loss conductors, and virtual array antennas. In 2014, he was the recipient of the Edward E. Altschuler Best Paper Prize from IEEE APS Magazine, and in 2016, the Best Paper Award from IEEE ANTEM. In 2017, he received the Booker Gold Medal for outstanding contributions to antenna miniaturization by electromagnetics and numerical techniques, small satellite terminals, planar antennas, invention of virtual reflectors, low loss engineered conductors and dielectric film components and antennas from the International Union of Radio Science, URSI. In 2018, he was a recipient of the IEEE Antennas and Propagation Society's Distinguished Achievement Award for the contributions to singular electromagnetics, moment methods, reflector feeds and virtual arrays, wideband antennas, gain enhancement in miniaturized antennas, and dielectric film circuits and antennas.